LAWRENCE
LIVERMORE
NATIONAL
LABORATORY

LLNL-PROC-656399

The Mesoscale Evolution of Voids in HMX-based Explosives During Heating Through the beta-delta Phase Transition

T. M. Willey, L. Lauderbach, F. Gagliardi, T. van Buuren, L. Glascoe, J. Tringe, J. R. I. Lee, K. Springer, J. Ilavsky

July 2, 2014

International Detonation Symposium
San Francisco, CA, United States
July 14, 2014 through July 18, 2014

Disclaimer

The Mesoscale Evolution of Voids in HMX-based Explosives During Heating Through the β-δ Phase Transition

Trevor M. Willey, Lisa Lauderbach, Franco Gagliardi, Tony van Buuren,
Libby Glascoe, Joe Tringe, Jonathan R. I. Lee, and Keo Springer
Lawrence Livermore National Laboratory, Livermore CA 94550

Jan Ilavsky
Argonne National Laboratory, Argonne IL

HMX-based explosives were heated through the β-δ phase transition. Ultra-small angle scattering, recorded as the HMX was heated indicate how the void volume and mesoscale structure of the explosive changes due to the phase transition. Molecular diffraction was simultaneously recorded to ascertain the phase of the HMX during the heating cycle. X-ray microtomography, performed before and after heating, shows the character of extensive microstructural damage at longer length scales caused by the temperature cycle and solid-state phase transition.

Introduction

HMX-based explosives heated through the β-δ phase transition exhibit increased sensitivity. HMX-based explosives also "cook-off" at elevated temperatures above this phase transition, when self-heating from exothermic reactions leads to deflagration and even detonation. The sensitivity is qualitatively attributed to two factors: the lower thermal stability of the δ-phase[1], as well as increased hot spots[2] and initiation centers from voids and porosity created during the phase transition. Quantification of the affect of how mesoscale (~10nm to ~1 um) voids affects sensitivity requires experimental measurement of such porosity during heating to address open questions regarding physiochemical processes that govern HMX sensitivity[1].

Inhomogeneities in electron density give rise to small angle scattering. Small angle X-ray scattering (SAXS) is sensitive to structural inhomogeneities with dimensions between ~ 1nm and 5 μm and, as such, is ideally suited to studying the size and size dispersion of voids in high explosives. A comprehensive treatment of the theoretical basis for obtaining this information from a scattering profile lies beyond the scope of this paper and can be found elsewhere in the literature[3]. Nonetheless, we present a brief overview of the key processes and equations that define the scattering profile.

In its simplest form, the scattered intensity is the square of the Fourier transform of the scattering length density: $\rho(\mathbf{r})$

$$I(q) = \left| \int \rho(\mathbf{r}) e^{-iq\mathbf{r}} \, d\mathbf{r} \right|^2 \quad (1)$$

where $q = \frac{4\pi}{\lambda}\sin(\theta)$, with λ as the wavelength of scattered radiation, and θ is the scattering half angle. The scattering density in a unit cell can be represented by a scattering density

function $\rho_u(\mathbf{r})$; the spatial distribution of the scattering sights is given by $z(\mathbf{r})$. The total scattering length density is a convolution of these two terms: $\rho(\mathbf{r}) = \rho_u(\mathbf{r}) * z(\mathbf{r})$. This leads to the scattering intensity: $I(q) \propto f(q)S(q)$, where $f(q)$, the general scattering form factor, arises from $\rho_u(\mathbf{r})$, and the structure factor $S(q)$ comes from $z(\mathbf{r})$. Assuming dilute voids with uncorrelated positions and random orientation, $S(q)$ is constant equal to unity, and the scattering is only a function of the form factor. In this approximation, scattering can be written in the following form:

$$I(q) = |\Delta\rho|^2 \int_0^\infty |F(q,s)|^2 V^2(s) NP(s)\, ds \quad (2)$$

In Eq. 2, s is the size of the scattering particle, $\Delta\rho$ is the scattering contrast (related to the difference in electron density) between the scatterer and its surroundings, $F(q,s)$ is the scattering form factor, $V(s)$ is the volume of the particle, N is the total number of particles, and $P(s)$ is the probability of having a scatterer of size s (the scattering size distribution function).

Although $\rho(\mathbf{r})$ gives a unique scattering intensity profile, the inverse is not unique. Therefore, eq. 2 must be used to generate the scattering based on an assumed form factor and size distribution of particles. For this study, the voids were modeled using a form factor for spheres. Furthermore, we assumed that the voids were randomly and uniformly dispersed throughout the explosive.

To quantify mesoscale changes influencing sensitivity, we performed USAXS/SAXS on HMX-based LX-10 (95% HMX, 5% Viton), PBX-9501 (95% HMX, 5% Estane and BDNPA-F), and single crystals of HMX at elevated temperatures. Only LX-10 data is shown for brevity. The materials were pressed between 0.7 and 0.8 mm thick, and subsequently laser-cut to about 2.0 mm in diameter, leading to sample masses of about 10 mg. A Linkam THMS600 modified for x-ray scattering was used to heat and control the temperature of the explosive. The experiments were performed at 15-ID-D at the Advanced Photon Source at Argonne National Laboratory using the upgraded USAXS instrument[4]. Data were analyzed using the Irena and Indra SAXS reduction and analysis codes[5]. These measurements, during heating, contrast previous studies that acquired SAXS after returning HMX-based samples to ambient temperatures[6, 7]. X-ray computed tomography performed at beamline 8.3.2 at the Advanced Light Source was also used to investigate the internal damage in the explosives.

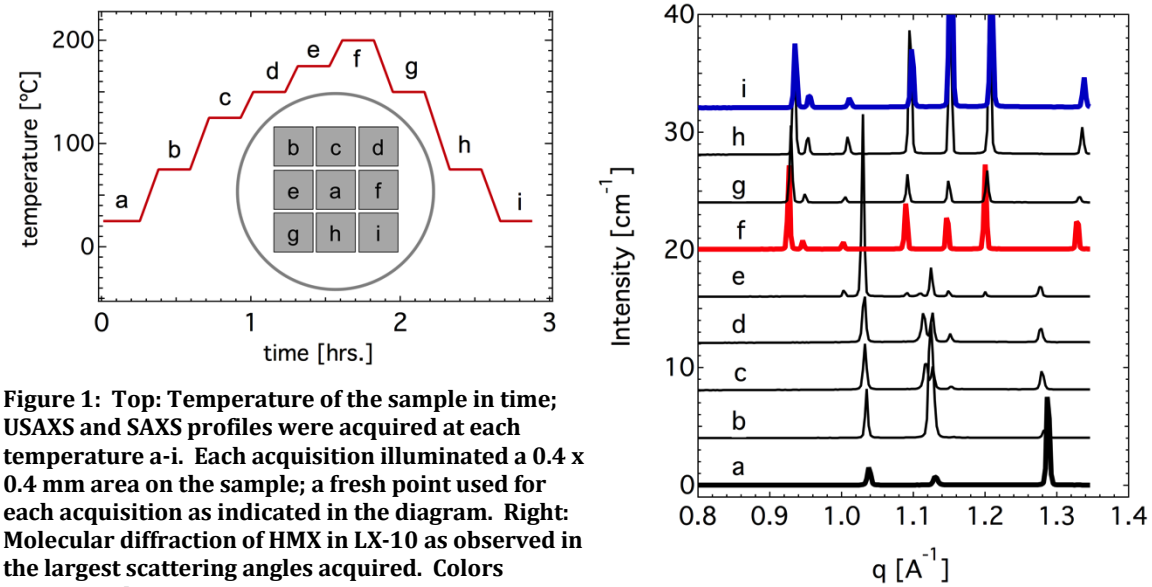

Figure 1: Top: Temperature of the sample in time; USAXS and SAXS profiles were acquired at each temperature a-i. Each acquisition illuminated a 0.4 x 0.4 mm area on the sample; a fresh point used for each acquisition as indicated in the diagram. Right: Molecular diffraction of HMX in LX-10 as observed in the largest scattering angles acquired. Colors correspond to acquisitions in Fig. 2.

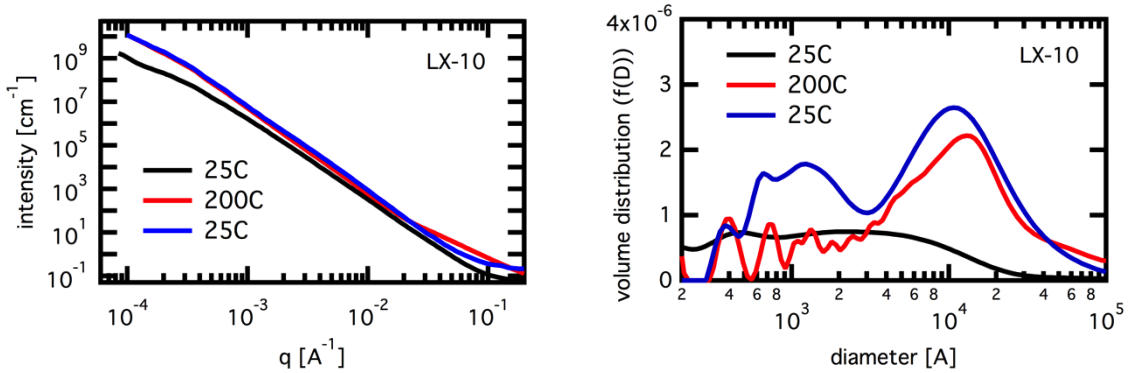

Figure 2: Ultra-small angle x-ray scattering (USAXS) from LX-10 during heating (left) and rudimentary void volume distributions derived directly from the USAXS.

Results and Discussion

The temperature profile used in these studies and beam positions on the sample are depicted in Figure 1. Sample temperature was held constant during USAXS and SAXS acquisitions and ramped between scans at the rate indicated. Concurrent to mesoscale porosity measurements in the USAXS, the SAXS, with sufficiently high scattering angle, monitors the phase of the HMX in LX-10 through molecular diffraction peaks. Although peak intensities may vary as HMX crystallites have varying average orientations in each sample point, the diffraction shows the solid-solid β-δ phase transition[8, 9] occurs between acquisitions e and f, as the temperature is ramped from 175 to 200C. Further, the explosive remains in the δ phase when cooled back to room temperature during this cycle .

Figure 2 presents the USAXS (left) and USAXS-derived void volume distributions[5] (right.) Three acquisitions at positions a, f, and i (Fig. 1) at temperatures of 25C, 200C, and 25C are presented for clarity. Care was taken to quantify and avoid x-ray induced changes to the scattering; we noted increased sensitivity to such damage at elevated temperatures (not shown). The USAXS, sensitive to scattering from objects or voids ~10 nm to ~5 *u*m, shows relatively stable LX-10 mesoscale structure upon heating from 25C to about 175C. A dramatic scattering change occurs promptly with the β-δ phase transition. Scattering is greater throughout the entire q-range in all scans after the transition as depicted in 200C and later 25C δ- phases, particularly at low (~10^{-4}) and high (10^{-1} Å^{-1}) q-ranges. This increased scattering implies a dramatic increase in void volume within the material. USAXS-derived void volume[5] starts at 1.3%, hits 7% at 200C, and increases to 8% after cooling back to 25C. The power law slope at ~5x10^{-3} Å^{-1} is most shallow prior to heating (-3.7), while heated samples are slightly higher. While this slope does not unambiguously give morphology information, it does indicate that the low-q scattering centers either possess surface texture, have 2D or 1D morphological characteristics, or have a broad size distribution extending towards smaller sizes. Similar features were observed in PBX-9501 and single-crystal HMX.

Microtomography (Fig. 3) performed before and after USAXS experiments, shows extensive cracking in the sample. Note that tomography acquisitions were acquired several days before, and several days after the USAXS/SAXS acquisition, and the post-temperature cycle sample, after several days, has likely reverted to the β phase. The observed cracking occurs primarily but not exclusively at crystallite boundaries at larger (>5 μm) length scales. The slices before and after heating could not be registered, even with fiducials placed on the samples. The lack of similarity in the tomography data before and after heating indicates extensive changes occur in mm-scale crystallite morphology during the temperature cycle.

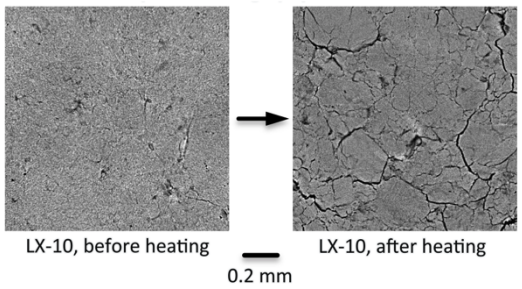

Figure 3: X-ray microtomography slice from LX-10 before and after heating. Cracking occurs throughout the sample.

Summary and Conclusions

Small-angle scattering shows the most dramatic change in porosity occurs promptly with the β-δ phase transition with a large increase (in this case from ~1.3% to ~7%) in mostly micron-scale porosity. These results are key to quantifying how the β-δ phase change damages HMX crystallites, and how new porosity affects the sensitivity of HMX at elevated temperatures providing quantitative mesoscale structural changes that are due to the phase transition.

Acknowledgements:

The authors thank I. Tran, LLNL, for assistance during USAXS experiments, and D. Parkinson, ALS, LBNL, for assistance during tomography experiments. This research was partially supported by the Joint DoD-DOE Munitions Technology Development Program. This work was performed under the auspices of the U.S. Department of Energy by Lawrence Livermore National Laboratory under Contract DE-AC52-07NA27344. ChemMatCARS Sector 15 is supported by the National Science Foundation/Department of Energy under grant number NSF/CHE-1346572. Use of the Advanced Photon Source, an Office of Science User Facility operated for the U.S. Department of Energy (DOE) Office of Science by Argonne National Laboratory, was supported by the U.S. DOE under Contract No. DE-AC02-06CH11357. The Advanced Light Source is supported by the Director, Office of Science, Office of Basic Energy Sciences, of the U.S. Department of Energy under Contract No. DE-AC02-05CH11231.

References:

1. Sharia, O., R. Tsyshevsky, and M.M. Kuklja, *Surface-Accelerated Decomposition of delta-HMX.* Journal of Physical Chemistry Letters, 2013. **4**(5): p. 730-734.
2. Hatano, T., *Spatiotemporal behavior of void collapse in shocked solids.* Physical Review Letters, 2004. **92**(1): p. 015503.
3. Glatter, O. and O. Kratky, eds. *Small Angle X-ray Scattering*. 1982, Academic Press Inc.: London. 515.
4. Ilavsky, J., et al., *Ultra-small-angle X-ray scattering at the Advanced Photon Source.* Journal of Applied Crystallography, 2009. **42**: p. 469-479.
5. Ilavsky, J. and P.R. Jemian, *Irena: tool suite for modeling and analysis of small-angle scattering.* Journal of Applied Crystallography, 2009. **42**(42): p. 347-353.
6. Peterson, P.D., J.T. Mang, and B.W. Asay, *Quantitative analysis of damage in an octahydro-1,3,5,7-tetranitro-1,3,5,7-tetrazonic-based composite explosive subjected to a linear thermal gradient.* Journal of Applied Physics, 2005. **97**: p. 093507.
7. Yan, G.Y., et al., *A small-angle X-ray scattering study of micro-defects in thermally treated HMX.* Acta Physica Sinica, 2012. **61**(13).
8. Saw, C.K. in *The 12th International Detonation Symposium.* 2002. San Diego, CA.
9. Xue, C., et al., *The beta-delta-Phase Transition and Thermal Expansion of Octahydro-1,3,5,7-Tetranitro-1,3,5,7-Tetrazocine.* Propellants Explosives Pyrotechnics, 2010. **35**(4): p. 333-338.